Vol. 11: 11–19, 1996 | AQUATIC MICROBIAL ECOLOGY Aquat Microb Ecol | Published August 29

CO_2 production predicted from isocitrate dehydrogenase activity and bisubstrate enzyme kinetics in the marine bacterium *Pseudomonas nautica*

T. Packard[1,*], E. Berdalet[2], D. Blasco[3], S. O. Roy[1], L. St-Amand[1], B. Lagacé[1], K. Lee[1], J.-P. Gagné[4]

[1]Institut Maurice-Lamontagne, CP 1000, Mont-Joli, Québec, Canada G5H 3Z4
[2]Institut de Ciencias Marinas, Passeig Juan Borbó c/n, E-08030 Barcelona, Spain
[3]329 Rte 298 Sud, St-Donat de Rimouski, Québec, Canada G0K 1L0
[4]Département d'Océanologie, Université du Québec à Rimouski, 300 allée des Ursulines, Rimouski, Québec, Canada G5L 3A1

ABSTRACT: CO_2 production in aerobic bacteria was modeled from the time-courses of the *in vitro* activity of isocitrate dehydrogenase (IDH), bacterial protein, and the concentration of the carbon source in the cultures. The model was based on the concept of bisubstrate control of the IDH reaction throughout the exponential, steady-state, and senescent phases of the cultures. In the exponential phase, the measured rates of CO_2 production and the *in vitro* IDH activity were closely coupled, but in the senescent phase, they became uncoupled. The *in vitro* IDH activity remained high even after the culture's carbon source was exhausted, while the CO_2 production fell to low levels. Based on the hypothesis that this uncoupling was caused by internal substrate limitation, 2 mathematical models incorporating a bisubstrate enzyme kinetics algorithm were constructed and tested. The models predicted the rate of CO_2 production throughout the different phases of the cultures with an r^2 greater than 0.84.

KEY WORDS: Respiration · Metabolism · Bacteria · Carbon dioxide · Ocean model · Isocitrate dehydrogenase activity

INTRODUCTION

Impending global climate change driven by greenhouse warming has intensified the need to understand and measure the temporal and spatial variability of biogeochemical processes in the ocean (Golden 1989). The respiratory CO_2 production rate (R_{CO_2}) in the ocean is one of these processes that, if better known, would improve global estimates of new production and deep-ocean CO_2 sequestering. Currently, measurements of R_{CO_2} can be made on individual aquatic organisms and cultures of microorganisms where rates greater than 1 µmol CO_2 min^{-1} l^{-1} prevail, but R_{CO_2} cannot be measured in seawater from oceanic regions and certainly cannot be measured at rates needed for mesoscale oceanographic studies (Zirino 1985, Savenkoff et al. 1995). Since the respiratory R_{CO_2} is controlled by the decarboxylases associated with the Krebs cycle (Hurley et al. 1991), we intuited that these enzymes could serve as bioindices of R_{CO_2} and have begun to investigate their potential in predicting R_{CO_2} in marine bacteria.

The CO_2 produced by aerobically growing bacteria is largely the result of 5 enzymes, isocitrate dehydrogenase (IDH), α-ketoglutarate dehydrogenase (KGDH), pyruvate dehydrogenase (PDH), malic enzyme (ME), and phosphoenolpyruvate carboxykinase (PEPCK; Walsh & Koshland 1984, Holms 1986a, b). Of these, IDH is in a unique position to exert metabolic control, because it links the Krebs cycle to the respiratory electron transfer system (Bennett & Holms 1975,

*E-mail: t_packard@qc.dfo.ca

Hurley et al. 1990a, b, 1991). Furthermore, IDH is activated and inactivated by IDH kinase/phosphatase (LaPorte & Koshland 1982, Nimmo & Nimmo 1984) suggesting that IDH activity and R_{CO_2} could exhibit a coupling throughout the different growth phases of the bacterial culture. Here, we characterize this coupling of IDH with R_{CO_2} in batch cultures of the marine bacterium *Pseudomonas nautica*.

This study first tested the concept that R_{CO_2} is a linear function of the *in vitro* activity of IDH (A_{IDH}). Finding this concept inadequate, the investigation tested the concept that R_{CO_2} is a function of the *in vivo* activities of IDH (V_{IDH}) and associated decarboxylases. This part of the investigation involved mathematical modeling. A simple IDH model based on simulated V_{IDH} and its empirical relationship with R_{CO_2} was constructed and compared with a complex model based on the 5 decarboxylases mentioned above.

Time-series experiments with batch cultures of *Pseudomonas nautica* were run. R_{CO_2}, A_{IDH}, bacterial protein, and pyruvate were measured throughout the exponential, steady state, and senescence phases of these cultures. Uncoupling between A_{IDH} and R_{CO_2} in the senescent phase became obvious. Algorithms were developed to predict V_{IDH} and to calculate the total *in vivo* enzymatic CO_2 production rate (V_{CO_2}). These algorithms were based on the ideas that senescent-phase uncoupling between A_{IDH} and R_{CO_2} was caused by substrate limitation of IDH, that bisubstrate enzyme kinetics could predict V_{IDH} from A_{IDH}, and that V_{CO_2} was a linear function of V_{IDH} or was the sum of the *in vivo* activity of all 5 decarboxylases. To test these ideas, time functions of the IDH substrates (isocitrate and $NADP^+$) were modeled from pyruvate and protein time-course data. Then, from these substrate models, from the V_{IDH} model, and from the A_{IDH} time course, the V_{CO_2} time profile was computed. These V_{CO_2} computations compared favorably with the measured R_{CO_2} time profiles.

MATERIALS AND METHODS

Experimental design. To investigate the degree of association between A_{IDH} and R_{CO_2} in different bacterial growth stages, time-profile experiments (1 or 14 d) were run on batch cultures, maintained on pyruvate at 22°C. Samples were taken for pyruvate, protein, A_{IDH}, and R_{CO_2} as the cultures passed through exponential growth, steady state and senescence. The results from two 1 d experiments and one 14 d experiment are presented.

Bacteria cultures. *Pseudomonas nautica* (Strain 617), an oil degrading bacterium isolated from the Gulf of Fos, France (Bonin 1986, Bonin et al. 1987a, b), was cultivated aerobically at 22°C in a phosphate-buffered medium (0.33 mM, pH 7.5) containing 400 mM NaCl, 10 mM $MgSO_4 \cdot 7H_2O$, 10 mM $CaCl_2 \cdot 2H_2O$, 10 mM KCl, 25 mM NH_4Cl, 0.01 mM $FeSO_4 \cdot 7H_2O$, and 20 mM pyruvate. The original culture was kindly given to us by Dr P. Bonin of the University of Aix-Marseille. Growth was monitored from absorbance at 550 nm (OD550). OD550 and protein (M) were related by the regression equation $M = 221.8\,OD550 - 19.9$ (n = 21). This relationship held for all culture phases with an r^2 of 0.987 ($p < 0.001$).

Respiration measurements. R_{CO_2} (µmol CO_2 min^{-1} l^{-1}) was measured in duplicate with a Micro-Oxymax respirometer according to Varma & Palsson (1994) and Berdalet et al. (1995). The standard error was 1.3% (n = 18).

Biochemical sampling. Samples (5 to 10 ml) of the bacteria culture were centrifuged for 15 min at 10000 × *g* at 4°C. A sample of the supernatant fluid was immediately transferred to an acid rinsed cryovial and stored in liquid nitrogen for pyruvate analysis. Pellets of concentrated bacteria were resuspended in 2 ml of the IDH-extraction buffer [25 mM MOPS (pH 7.5) and 167 mg ml^{-1} lysozyme] for IDH analyses, and in 2 to 4 ml 1 N NaOH (at 20°C) for protein analysis. All samples were stored in liquid nitrogen according to Ahmed et al. (1976).

Pyruvate measurements. Pyruvate in the supernatant fluid was measured in its acid form at 210 nm by HPLC as described by Berdalet et al. (1995). Measurements were made in duplicate; the standard error was 1.2% (n = 10).

***In vitro* IDH activity (A_{IDH}).** A_{IDH} was assayed photometrically by following the NADPH production at 340 nm (Reeves et al. 1969, 1972, Holms & Bennett 1971, Berdalet et al. 1995). The assay is based on the reaction, ISO + $NADP^+ \leftrightarrow$ α-KG + NADPH + CO_2, where ISO and α-KG represent isocitrate and α-ketoglutarate. Results are reported as µmol CO_2 $(min)^{-1}$ (liter of culture)$^{-1}$. Each data point represents 4 analyses (see Figs. 1 & 2). The standard error was 1.1% (n = 21).

Protein measurements. Protein in the bacterial pellet was analyzed by the Lowry method (Lowry et al. 1951) and reported as mg protein (liter of culture)$^{-1}$. Bovine Serum Albumen (BSA) was used as a standard. Each data point represents 4 analyses (see Figs. 1 & 2). The standard error was 0.7 % (n = 21).

Modeling computation. Modeling was done on a Macintosh IISi computer using the software Data Desk®, version 4.2, from Data Description Inc., Ithaca, NY. The merit of the isocitrate and $NADP^+$ algorithms was judged on their ability to generate declining time-profiles of isocitrate and $NADP^+$ within the boundary conditions of 1 to 60 µM (White et al. 1964, Lehninger 1970, Lehninger et al. 1993). The merit of the V_{IDH} algorithm was judged on the correlation (r^2) between the V_{IDH} and R_{CO_2} time profiles.

RESULTS

Time profiles of R_{CO_2}, A_{IDH}, protein, and pyruvate

The time-profile observations in the bacteria cultures during Expts A, B, and C are shown in Figs. 1 & 2. The pyruvate in the culture medium in the 3 experiments decreased from an initial level of 20 mmol l^{-1} to nearly zero within 24 h. Protein increased as an inverse image of the pyruvate decline from about 10 mg l^{-1} at the beginning to about 280 mg l^{-1} at the end of the experiments (Fig. 1).

The time course of the pyruvate (P) decrease in Expt A (Fig. 1A) was described by the equation:

$$P(t) = [P_0/(1 + e^{\mu(t-\phi)})] + P_f \quad (1)$$

where P_0 is the initial pyruvate level (20 µmol l^{-1}), P_f is the final pyruvate level (0.11 µmol l^{-1}), μ is culture growth rate (0.47 divisions h^{-1}), t is the time in hours, and ϕ is time of pyruvate exhaustion (12.7 h). Eq. (1) predicted the observed pyruvate decrease well; the regression equation between the modeled pyruvate (P) and the measured pyruvate (X) was $P = 1.00X + 0.084$ ($r^2 = 0.997$).

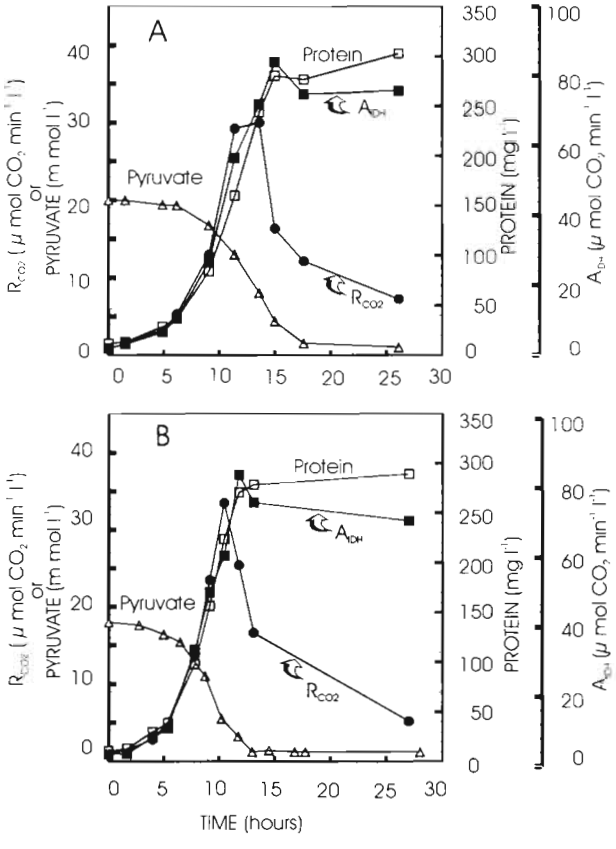

Fig. 1. Replicate 1 d time-course experiments (A & B) showing observations of A_{IDH}, R_{CO_2}, protein, and pyruvate. The analytical errors are given in the 'Materials and methods'

Table 1. R_{CO_2}-A_{IDH} and R_{CO_2}-M relationships by linear regression analysis on the exponential-phase data from Expts A & B. The A_{IDH}-M regression analysis was run on the data from all 3 growth phases of Expts A & B (data are shown in Fig. 1). Slope of the regression equation (m) and its intercept (b) are given with their standard errors

Function	m	b	n	r^2
$R_{CO_2} = f(A_{IDH})$	0.53 ± 0.02	−0.45 ± 0.67	11	0.984
$R_{CO_2} = f(M)$	0.16 ± 0.08	−0.50 ± 0.84	11	0.978
$A_{IDH} = f(M)$	0.28 ± 0.01	0.86 ± 1.90	21	0.974

The time course of the protein (M) increase in Expt A (Fig. 1A) was described by :

$$M(P) = M_0 + \gamma(P_\alpha - P) \quad (2)$$

where M is the bacterial protein, M_0 is the observed protein immediately after inoculation (11.6 mg protein l^{-1} for Expt A), γ is the yield of bacterial protein when all the pyruvate has been consumed [15.7 mg protein (mmol pyruvate)$^{-1}$ for Expt A], P is the pyruvate level from Eq. (1), and P_α is P at $t = 0$ (from Eq. 1). Note that since $P = f(t)$ and $M = f(P)$, Eq. (2) is also a time function. The regression equation between the modeled protein (M) and the measured protein (X) was $M = 1.00X - 12.58$ ($r^2 = 0.965$).

The time course of the A_{IDH} increase in both experiments followed the protein time course throughout all phases of growth. The regression between the 2 variables is given in Table 1.

The R_{CO_2} time profiles did not follow the A_{IDH} and protein time profiles over the life span of the cultures (Table 1, Figs. 1 & 2). In exponential growth, A_{IDH} and R_{CO_2} were in parallel and highly correlated (Table 1), but in senescence during pyruvate limitation, A_{IDH} and R_{CO_2} diverged. This divergence was especially apparent in Expt C where even after 13 d of nutrient depletion, A_{IDH} maintained at least 50% of its maximum activity whereas R_{CO_2} had fallen to less than 5% of its maximum value (Fig. 2).

Respiration models

The experimental results (Figs. 1 & 2) indicate clearly that R_{CO_2} cannot be predicted in a simple linear fashion by changes in A_{IDH} alone. If changing IDH concentrations ($\approx A_{IDH}$) were the important regulatory mechanism for R_{CO_2} in *Pseudomonas nautica*, then A_{IDH} would have declined along with R_{CO_2} in senescence. Since A_{IDH} did not decline, an alternative hypothesis was needed to explain the observations. If R_{CO_2} were regulated through changes in the *in vivo* IDH activity (V_{IDH}), then a decline in the intracellular isocitrate and

Table 2. Parameters and constants used in the pyruvate and protein Eqs. (1 & 2) and in the simple IDH and 5 enzyme models (Table 3) to predict V_{CO_2} (Figs. 4 to 6) from observations in Expt A (Fig. 1A)

Parameter	Value	Units
a	1.3×10^{-2}	(mmol pyruvate l^{-1})$^{-1}$
b	4.3×10^{-5}	(mg protein l^{-1})$^{-1}$
χ	0.19	
δ	8.76×10^{-4}	µmol NADP$^+$ (mmol pyruvate)$^{-1}$
ϕ	12.72	h
γ	15.7	mg protein (mmol pyruvate)$^{-1}$
η	5.9×10^{-7}	µmol isocitrate (mg protein)$^{-1}$
K_{ia}	42.8	µmol
K_{ISO}	8.75	µmol isocitrate
K_{NADP^+}	18.0	µmol NADP$^+$
λ	4.44×10^{-4}	µmol isocitrate (mmol pyruvate)$^{-1}$
μ	0.471	divisions h^{-1}
M_0	11.7	mg protein l^{-1}
ν	1.2	
P_σ	20.06	mmol pyruvate l^{-1}
P_f	0.11	mmol pyruvate l^{-1}
P_0	20.00	mmol pyruvate l^{-1}
Q	8.17×10^{-7}	mmol pyruvate (mg protein)$^{-2}$ l^{-1}
θ	2.05×10^{-5}	(mg protein l^{-1})$^{-1}$
σ	7.6×10^{-3}	h^{-1}
υ	1.51	mmol pyruvate l^{-1}
ω	5.2×10^{-5}	µmol NADP$^+$ (mg protein)$^{-1}$
ψ	7.32×10^{-3}	(mg protein l^{-1})$^{-1}$
ζ	8.32×10^{-2}	(mmol pyruvate l^{-1})$^{-1}$

NADP$^+$ pools falling in parallel with the declining extracellular pyruvate (Fig. 1) would reduce V_{IDH} in senescence even though A_{IDH} remained high. Such a hypothesis would predict a lower V_{IDH} to A_{IDH} ratio, or a lower value of its physiological expression, R_{CO_2}/A_{IDH}, in senescence than in exponential growth. The observations support this hypothesis. R_{CO_2}/A_{IDH} ranged from 0.095 to 0.006 during senescence (Fig. 1) while during exponential growth it was 0.53 ± 0.02 (Table 1).

Stronger support for this hypothesis would be a demonstration of how A_{IDH} could be modulated by enzyme kinetics to give a V_{IDH} time course that moved in parallel with the measured R_{CO_2} time course. Here we demonstrate how this can be done by developing 2 respiration models based on the data of Expt A.

To simulate the V_{IDH} time course from the A_{IDH} measurements in Expt A one needs to consider bisubstrate enzyme kinetics because 2 substrates (NADP$^+$ and isocitrate) are the required reactants in the IDH catalyzed reaction (Hurley et al. 1991, Kuby 1991). The following equation in which $V_{IDH} = f(A_{IDH})$ can be written to describe the IDH reaction:

$$V_{IDH} = \frac{\nu A_{IDH}}{1 + \left(\frac{K_{ISO}}{[ISO]}\right) + \left(\frac{K_{NADP^+}}{[NADP^+]}\right) + \left(K_{ia} K_{NADP^+}/[ISO][NADP^+]\right)} \quad (3)$$

Here, K_{ISO} and K_{NADP^+} are bisubstrate-Michaelis constants for isocitrate and NADP$^+$ (Mahler & Cordes 1971, Kuby 1991), K_{ia} is the dissociation constant for the enzyme-isocitrate complex, and [ISO] and [NADP$^+$] are the substrate concentrations (Table 2). In the 2 models developed in this paper the enzyme activities (V_{IDH} and A_{IDH}) are normalized by culture volume and both are functions of time (Fig. 1). Thus A_{IDH} in Eq. (3) is not a constant; it was measured as a time function (Fig. 1), but it also equals MV_{max}, where V_{max} is the maximal velocity of IDH and M is the protein from Eq. (2). ν is a unitless scaling factor that reflects an enzyme assay's underestimation of V_{max}: Walsh & Koshland's (1984) value of 1.2 is used here for ν.

From the conceptual model that $R_{CO_2} = f(V_{IDH})$ and that V_{IDH} can be calculated from Eq. (3), 2 models of CO_2 production were developed. The first model was based on the isocitrate and NADP$^+$ time profiles (Fig. 3) which were modeled from Eqs. (1 & 2) for the pyruvate and protein time profiles and from the empirical relationship between R_{CO_2} and V_{IDH} throughout the time

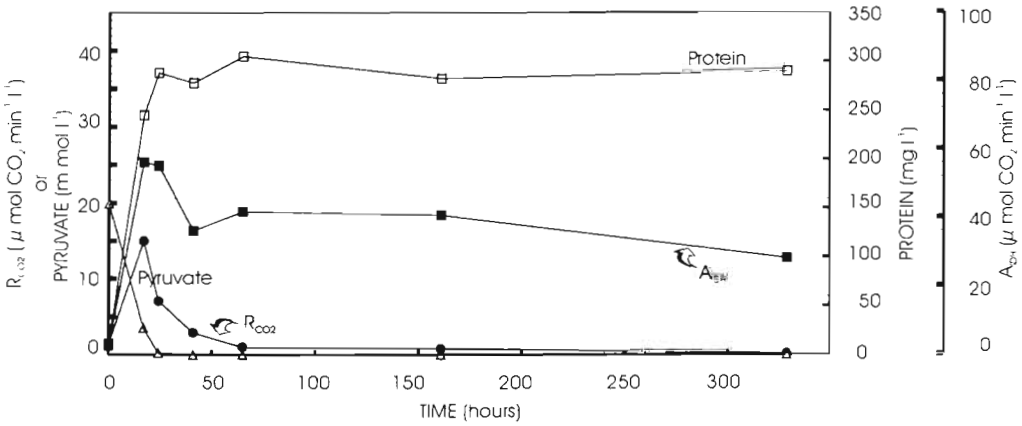

Fig. 2. 14 d time-course of A_{IDH}, R_{CO_2}, protein, and pyruvate (Expt C)

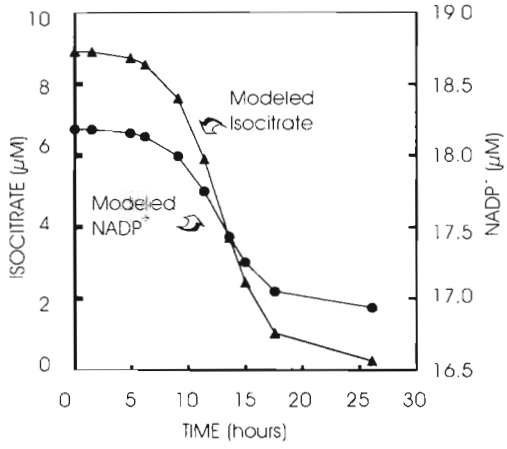

Fig. 3. Simulated isocitrate and $NADP^+$ concentrations from Eqs. (4 & 5) for Expt A

course of Expt A (Fig. 4B). The second, more complex model computes V_{IDH} as in the first model, but replaces the empirical relationship between R_{CO_2} and V_{IDH} by a simulation of the contribution to R_{CO_2} by the *in vivo* activity of the 4 other decarboxylases, namely, V_{KGDH}, V_{PDH}, V_{ME}, and V_{PEPCK}.

IDH model

If the low R_{CO_2} in senescence is caused by substrate limitation, then Eq. (3) should predict the shape of the R_{CO_2} versus time curve throughout the exponential, steady state, and senescent phases of the bacteria culture. To test this we need values of K_{ISO}, K_{NADP^+}, K_{ia} and the time courses of isocitrate and $NADP^+$. The Michaelis constants, K_{ISO} and K_{NADP^+}, for bacteria range from 0.4 to 250 μM for isocitrate, and 0.3 to 27 μM for $NADP^+$ (Walsh & Koshland 1984, Chen & Gadal 1990). For our model we set K_{ISO} equal to 8.75 μM and K_{NADP^+} equal to 18.0 μM (Table 2). These values are similar to those used by Hurley et al. (1990a, b, 1991). K_{ia} has not been measured in bacteria, so we set it to 42.8 μM through optimization. The concentrations of isocitrate and $NADP^+$ were made functions of both pyruvate in the growth media (P) and the bacterial protein (M). Isocitrate concentrations between the boundary conditions, 8.9 and 0.62 μM (Fig. 3), are predicted from the equation:

$$ISO(P, M) = \lambda P + \eta M \quad (4)$$

where λ is 4.44×10^{-4} μmol isocitrate (mmol pyruvate)$^{-1}$ and η is 5.9×10^{-7} μmol isocitrate (mg protein)$^{-1}$. $NADP^+$ concentrations between the boundary conditions, 18.13 and 16.58 μM (Fig. 3), are predicted from the equation:

$$NADP^+(P, M) = \delta P + \omega M \quad (5)$$

where δ is 8.76×10^{-4} μmol $NADP^+$ (mmol pyruvate)$^{-1}$ and ω is 5.2×10^{-5} μmol $NADP^+$ (mg protein)$^{-1}$. Fig. 3 shows the time courses of these functions for Expt A. Note that they both resemble the pyruvate time course (Fig. 1A). The algorithms for pyruvate and protein (Eqs. 1 & 2) were used in Eqs. (4 & 5) to calculate the isocitrate and $NADP^+$ time functions (Fig. 3). Because Eqs. (1 & 2) represent the original protein and pyruvate measurements so well, using either Eqs. (1 & 2) or using the original data (Fig 1) changes the calculation of isocitrate and $NADP^+$ very little.

When the isocitrate and $NADP^+$ functions (Eqs. 4 & 5) and the values of K_{ISO}, K_{NADP^+}, and K_{ia} (given above) are used in Eq. (3), V_{IDH} ranges from 0.3 μM min^{-1} l^{-1} at the beginning of Expt A to a maximum of 6.1 μM min^{-1} l^{-1} at 11.4 h (Fig. 4A). By the end of the experiment V_{IDH} has dropped to 0.9 mM min^{-1} l^{-1} From Fig. 4A one can see that throughout all phases of the bacteria culture, the V_{IDH} time course resembles the R_{CO_2} time course. A plot of V_{IDH} against R_{CO_2} (see Fig. 4B) in Expt A, shows a strong correlation ($r^2 = 0.877$) with a

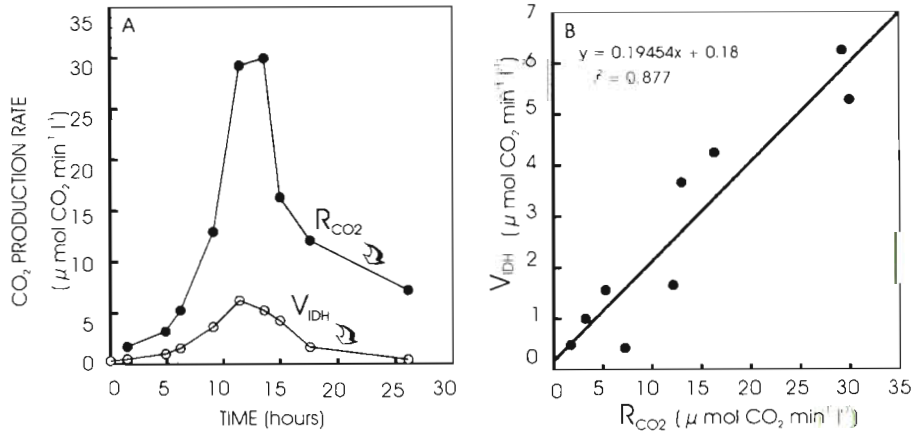

Fig. 4. (A) V_{IDH} generated from Eq. (3) counterpoised against the R_{CO_2} from Expt A. (B) V_{IDH} regressed against R_{CO_2}; slope is χ. All calculations based on data from Expt A

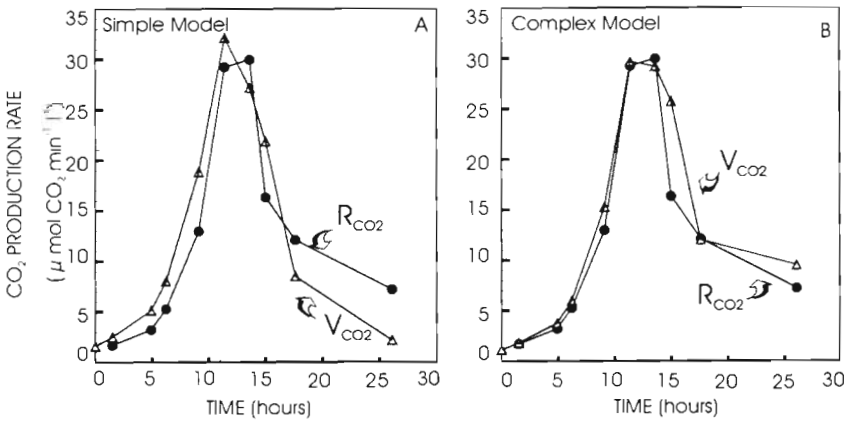

Fig. 5. For Expt A: correspondence between CO_2 production rate predicted by the models (V_{CO_2}) and measured CO_2 production rate (R_{CO_2}). Parameters used in the models are summarized in Table 2, equations are summarized in Table 3

V_{IDH} to R_{CO_2} ratio (slope) of 0.19. This leads to a calculation of $V_{CO_2} = f(V_{IDH})$ from the final algorithm of the simple IDH model, i.e.:

$$V_{CO_2} = V_{IDH}/\chi \quad (6)$$

where $\chi = V_{IDH}/R_{CO_2}$ and V_{CO_2} is the predicted rate of CO_2 production (as contrasted to R_{CO_2}). Fig. 5A shows the resemblance of V_{CO_2} to R_{CO_2}. The regression equation between V_{CO_2} and R_{CO_2}, for Expt A, is $V_{CO_2} = 1.001\,R_{CO_2} + 0.93$ ($n = 9$, $r^2 = 0.877$).

Five enzyme model

The simple IDH model, in spite of its ability to simulate the R_{CO_2} time course, simplifies the role of KGDH, PDH, ME, PEPCK to a constant, χ. A more realistic model would simulate the *in vivo* activity of these enzymes. To achieve this we developed a more complex model based on the equation:

$$V_{CO_2} = V_{IDH} + V_{KGDH} + V_{PDH} + V_{ME} + V_{PEPCK} \quad (7)$$

where V represents the *in vivo* activity of each decarboxylase in μmol min^{-1} (liter of culture)$^{-1}$ (Walsh & Koshland 1984). Algorithms for V_{KGDH}, V_{PDH}, V_{ME}, and V_{PEPCK} as functions of V_{IDH} are developed as follows.

V_{KGDH} is closely coupled to V_{IDH}. For *Escherichia coli* growing on glucose-6-phosphate, V_{KGDH} is 73% of V_{IDH}; for *E. coli* growing on acetate, V_{KGDH} is 94 to 95% of V_{IDH}. We developed a V_{KGDH} algorithm assuming that V_{KGDH} in *Pseudomonas nautica* behaves as it does in *E. coli*. The algorithm balances the effect of the pyruvate decrease against the protein increase so that the V_{KGDH} lags behind the V_{IDH} during growth on pyruvate but becomes equal to it when pyruvate exhaustion limits growth. Initially, V_{KGDH}/V_{IDH} is 0.74, at the maximum it is 0.84, and at the end of the experiment it is 1.0 (Fig. 6). This algorithm takes the form:

$$V_{KGDH}(V_{IDH}, P, M) = V_{IDH}(1 - aP - bM) \quad (8)$$

where the constants, a and b, equal 1.3×10^{-2} (mmol pyruvate $l^{-1})^{-1}$ and 4.3×10^{-5} (mg protein $l^{-1})^{-1}$, respectively.

The PDH algorithm (Eq. 9) is dictated by the requirement that V_{PDH} exceed V_{IDH} when the bacteria use glucose or pyruvate as a carbon source, because some carbon departs the Krebs cycle at the level of citrate to supply citrate lyase for fatty acid synthesis. Well-oxygenated glucose-grown cultures of *Escherichia coli* are characterized by a V_{PDH}/V_{IDH} ratio of 1.66 (Holms 1986a, b). After a culture exhausts its pyruvate and grows on acetate, the V_{PDH}/V_{IDH} ratio would be lower

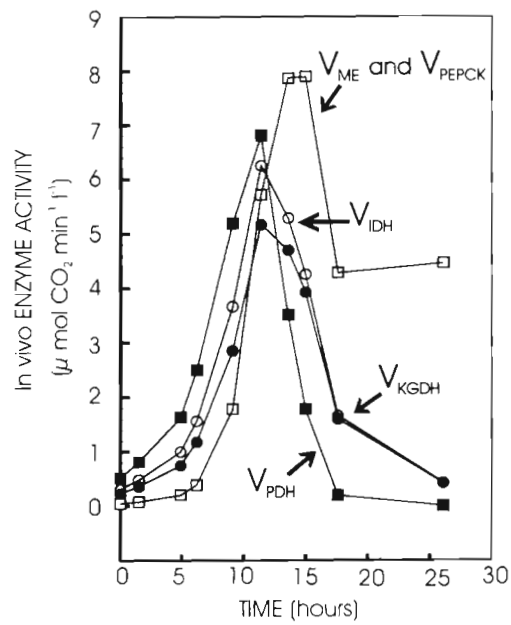

Fig. 6. *In vivo* activities of IDH, KGDH, PDH, ME, and PEPCK as calculated from Eqs. (3), (8), (9), and (10). The A_{IDH}, pyruvate, and protein data from which these curves were calculated are shown in Fig. 1A (Expt A). The modeled isocitrate and $NADP^+$ inputs for Eq. (3) are shown in Fig. 3. The sum of these activities from Eq. (7) (V_{CO_2}) is shown in Fig. 5B

than 1. We designed a function, based on the time courses of V_{IDH}, pyruvate, and protein in Expt A, that would fall off from the maximum faster than the V_{IDH} function (Fig. 6), but during exponential growth, while the medium still contains pyruvate, V_{PDH} would range from 1.66 to 1.28 × V_{IDH}. In senescence, V_{PDH} would be smaller than V_{IDH} (Fig. 6). This algorithm takes the form:

$$V_{PDH}(V_{IDH}, P, M) = V_{IDH}(\zeta P - \theta M - QM^2/P) \quad (9)$$

in which the constants are: $\zeta = 8.32 \times 10^{-2}$ (mmol pyruvate $l^{-1})^{-1}$, $\theta = 2.05 \times 10^{-5}$ (mg protein $l^{-1})^{-1}$, and $Q = 8.17 \times 10^{-7}$ (mmol pyruvate) (mg protein)$^{-2}$ l^{-1}.

V_{PEPCK} was set equal to V_{ME} as in the model of Walsh & Koshland (1984). The algorithm for ME (Eq. 10) was designed to increase V_{ME} after pyruvate depletion when the cells utilize excreted acetate (Holms 1986a, b). The algorithms for both enzymes generate low activities while pyruvate levels are high. This is consistent with the pyruvate inhibition of ME observed by Hsu et al. (1967). An important characteristic of these enzymes is that they retain *in vivo* activity in the senescent phase (Holms 1986a, b; Fig. 6). The resulting time course of the algorithm is shown in Fig. 6. The algorithm itself takes the form:

$$V_{ME}(V_{IDH}, P, M) = V_{PEPCK} = V_{IDH}e^{-\sigma t}(\psi M + \upsilon/P) \quad (10)$$

where $\psi = 7.32 \times 10^{-3}$ l (mg protein)$^{-1}$, $\upsilon = 1.51$ mmol pyruvate l^{-1} and $\sigma = 7.6 \times 10^{-3}$ h^{-1}.

Eq. (7), summing the *in vivo* activities of the 5 enzymes (Fig. 6), computes V_{CO_2}. This sum should equal R_{CO_2}. For Expt A, the time course for V_{CO_2} is shown in Fig. 5B. It simulates closely the R_{CO_2} time profile from Fig. 1A. When V_{CO_2} is plotted against R_{CO_2}, a 1:1 relation results ($V_{CO_2} = 0.998R_{CO_2} + 1.69$, n = 9) with $r^2 = 0.920$. This complex 5 enzyme model (Fig. 5B) predicts both the shape and the magnitude of the R_{CO_2} time course as well as the simple IDH model (Fig. 5A), but it does not invoke the empirical relationship between V_{IDH} and R_{CO_2} (χ). The equations for both models are summarized in Table 3.

DISCUSSION

Isocitrate dehydrogenase activity

The behavior of A_{IDH} in *Pseudomonas nautica* throughout different bacterial growth phases was unknown prior to this investigation. Would the absence of a carbon source signal the cell to dismantle surplus enzyme systems? Would the cell cannibalize its Krebs cycle enzymes and use the materials for other purposes, if there were no organic molecules to oxidize? Would IDH be inactivated by IDH kinase/phosphatase and kept in reserve, or would it be kept active but substrate limited? In reviewing recent research on the general question of maintaining enzymatic capacity during adverse conditions, Nystrom et al. (1990) found that most marine *Vibrio* strains remain metabolically active during starvation and are primed for substrate availability. For marine bacteria that inhabit an environment characterized by low but highly variable bioavailability of organic nutrients, this ability to maintain a reserve of alert-status enzymes would be important.

Table 3. Summary of equations used in both models. Each equation is a time function because it depends directly or indirectly upon the pyruvate time function (Eq. 1) and the A_{IDH} time course (Fig. 1). Note that $V_{PEPCK} = V_{ME}$. For the simple IDH model the first 6 equations are used. For the 5 enzyme model, all equations except Eq. (6) are used. Table 2 lists parameter values. Variable and parameters are defined in the text

Equation	Source in this paper: Eq. no.	Fig. no.
$P(t) = [P_0/(1 + e^{\mu(t - \phi)})] + P_I$	(1)	1
$M(P) = M_0 + \gamma(P_\alpha - P)$	(2)	1
$V_{IDH} = \dfrac{\nu A_{IDH}}{1 + \left(\dfrac{K_{ISO}}{[ISO]}\right) + \left(\dfrac{K_{NADP^+}}{[NADP^+]}\right) + \left((K_{ia}K_{NADP^+})/[ISO][NADP^+]\right)}$	(3)	4
$ISO(P, M) = \lambda P + \eta M$	(4)	3
$NADP^+(P, M) = \delta P + \omega M$	(5)	3
$V_{CO_2} = V_{IDH}/\chi$	(6)	5
$V_{CO_2} = V_{IDH} + V_{KGDH} + V_{PDH} + V_{ME} + V_{PEPCK}$	(7)	5
$V_{KGDH}(V_{IDH}, P, M) = V_{IDH}(1 - aP - bM)$	(8)	6
$V_{PDH}(V_{IDH}, P, M) = V_{IDH}(\zeta P - \theta M - QM^2/P)$	(9)	6
$V_{ME}(V_{IDH}, P, M) = V_{PEPCK} = V_{IDH}e^{-\sigma t}(\psi M + \upsilon/P)$	(10)	6

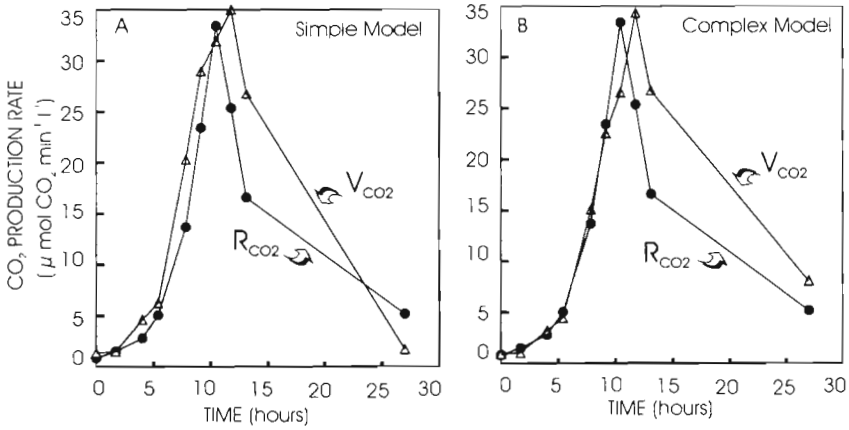

Fig. 7. Model simulations for Expt B (Fig. 1B). The correspondence between V_{CO_2} predicted by the (A) simple IDH and (B) complex 5 enzyme models and R_{CO_2} is given by the regression equation $V_{CO_2} = 1.19R_{CO_2} + 0.096$ ($r^2 = 0.89$) for the simple model and $V_{CO_2} = 0.99R_{CO_2} + 1.67$ ($r^2 = 0.84$) for the complex model

In our experiments, A_{IDH} tracked cellular protein throughout the exponential and steady states, and, to a lesser extent, the senescent phases (Table 1, Fig. 1). This suggests that IDH is constitutive in *Pseudomonas nautica*, that during starvation this enzyme is in alert status, and that it is not inactivated or degraded by IDH kinase/phosphatase after the culture's carbon source has been exhausted. It also suggests that A_{IDH} could serve as an index of living biomass in the absence of a protein measurement. When the A_{IDH} and protein data from both Expts A and B were pooled (Table 1) the regression equation was: $A_{IDH} = 0.28M + 0.86$ ($r^2 = 0.975$).

No simple linear equation could relate A_{IDH} to R_{CO_2} throughout all phases of the bacteria culture; A_{IDH} correlated well with R_{CO_2} only in the exponential growth phase (Fig. 1). The magnitude of A_{IDH} exceeded R_{CO_2} at all times, demonstrating the great capacity for CO_2 production at the enzyme level.

Reconstruction of the respiration rate

The reactions responsible for R_{CO_2} have long been identified, but the control of these reactions and their kinetics are still not well enough understood to allow quantitative reconstruction of the physiological respiration rate (R_{CO_2}). Rare is the account in the literature where either R_{CO_2} or R_{O_2} of whole cells or cultures is calculated from first principles and measurements of enzyme activities, substrate concentrations and biomass levels. In this paper we demonstrate how this might be done using Eqs. (4) to (9). We show that from the A_{IDH}, pyruvate and protein time-course data (Fig. 1A), one can simulate the physiological respiration rate (R_{CO_2}). The degree of success was high for Expt A (Fig 1); the r^2 values for the simple IDH and complex 5 enzyme models were 0.88 and 0.92.(Fig. 5)

Similar success was duplicated for an independent experiment, presented in Fig. 1B, Expt B. For this experiment, the measured values of P_0, M_0, and γ were 18 mmol pyruvate l^{-1}, 10 mg protein l^{-1}, and 16.2 mg protein (mmol pyruvate)$^{-1}$. When these values and the A_{IDH} data from Fig. 1B were entered into the 2 models (Table 3) and all other parameters held at the values listed in Table 2, R_{CO_2} was predicted with an r^2 value of 0.89 for the simple model and 0.84 for the complex model (Fig. 7). This success demonstrates the feasibility of using bisubstrate enzyme kinetics to predict the physiological respiration rate of a bacteria culture from 3 variables defining the culture's physiological state, namely, the enzyme potential (A_{IDH}), the biomass (M), and the level of its carbon source (P).

Acknowledgements. The Spanish Ministry of Science funded the post-doctoral fellowship to E.B. We thank J. Piuze, B. Sundby, and J. C. Therriault for their support and encouragement; A. Vézina for his constructive criticism; J. Brown for aid in the laboratory; and L. Devine-Castonguay for a careful review of the manuscript.

LITERATURE CITED

Ahmed SI, Kenner RA, King FD (1976) Preservation of enzyme activity in marine plankton by low-temperature freezing. Mar Chem 4:133–139

Bennett PM, Holms WH (1975) Reversible inactivation of the isocitrate dehydrogenase of *Escherichia coli* ML 308 during growth on acetate. J Gen Microbiol 87:37–51

Berdalet E, Packard T, Lagacé B, Roy S, St-Amand L, Gagné JP (1995) CO_2 production, O_2 consumption and isocitrate dehydrogenase in the marine bacterium *Vibrio natriegens*. Aquat Microb Ecol 9:211–217

Bonin P (1986) Nitrate reduction in simulated microniches by a denitrifying marine bacterium. Can J Microbiol 33: 276–279

Bonin P, Bertrand JC, Giordano G, Gilewicz M (1987a) Specific sodium dependence of a nitrate reductase in a marine bacterium. FEMS Microbiol Lett 48:5–9

Bonin P, Gilewicz M, Bertrand JC (1987b) Denitrification by a marine bacterium *Pseudomonas nautica* strain 617 Ann Inst Pasteur/Microbiol 138:371–383

Chen RD, Gadal P (1990) Structure, function and regulation of NAD and NADP-dependent isocitrate dehydrogenase in

higher plants and other organisms. Plant Physiol Biochem 28:411–427
Golden F (1989) The role of the seas in the planetary hothouse. Oceanus 32:2–3
Holms WH (1986a) The central metabolic pathways of *Escherichia coli*: relationship between flux and control at a branch point, efficiency of conversion to biomass, and excretion of acetate. Curr Top Cell Regul 28:69–105
Holms WH (1986b) Evolution of the glyoxylate bypass in *Escherichia coli*—an hypothesis which suggests an alternative to the Krebs cycle. FEMS Microbiol Lett 34: 123–127
Holms WH, Bennett PM (1971) Regulation of isocitrate dehydrogenase activity in *Escherichia coli* on adaptation to acetate. J Gen Microbiol 65:57–68
Hsu RY, Lardy HA, Cleland WW (1967) Pigeon liver malic enzyme: V. Kinetic studies. J Biol Chem 242:5315–5322
Hurley JH, Dean AM, Koshland DE Jr, Stround RM (1991) Catalytic mechanism of NADP-dependent isocitrate dehydrogenase, implications from the structures of magnesium isocitrate and NADP complexes. Biochemistry 30: 8671–8678
Hurley JH, Dean AM, Sohl JL, Koshland DE Jr, Stroud RM (1990a) Regulation of an enzyme by phosphorylation at the active site. Science 249:1012–1016
Hurley JH, Thorsness PE, Koshland DE Jr, Stroud RM (1990b) Regulation of isocitrate dehydrogenase by phosphorylation involves no long-range conformational change in the free enzyme. J Biol Chem 265:3599–3602
Kuby SA (1991) Enzyme catalysis, kinetics, and substrate binding. CRC Press, Boca Raton
LaPorte DC, Koshland DE Jr (1982) A protein with kinase and phosphatase activities involved in regulation of tricarboxylic acid cycle. Nature 300:458–460
Lehninger AL (1970) Biochemistry. The molecular basis of cell structure and function. Worth Publishers, New York
Lehninger AL, Nelson DL, Cox MM (1993) Principles of biochemistry. Worth Publishers, New York
Lowry OH, Rosebrough NJ, Farr AL, Randall RJ (1951) Protein measurement with the Folin phenol reagent. J Biol Chem 193:265–275
Mahler HR, Cordes EH (1971) Biological chemistry. Harper and Row, New York
Nimmo GA, Nimmo HG (1984) The regulatory properties of isocitrate dehydrogenase kinase and isocitrate dehydrogenase phosphatase from *Escherichia coli* ML308 and the roles of these activities in the control of isocitrate dehydrogenase. Eur J Biochem 141:409–414
Nystrom T, Flardh K, Kjelleberg S (1990) Responses to multiple-nutrient starvation in marine *Vibrio* sp. strain CCUG 15956. Bacteriol 172:7085–7097
Reeves HC, Daumy GO, Lin CC, Houston M (1972) $NADP^+$ specific isocitrate dehydrogenase of *Escerichia coli* I. Purification and characterization. Biochim Biophys Acta 258:27–39
Reeves HC, Rabin R, Wegener WS, Ajl SJ (1969) Assays of enzymes of the tricarboxylic acid and glyoxylate cycles. In: Norris JR (ed) Methods in microbiology. Academic Press, San Francisco
Savenkoff C, Vézina AF, Chanut JP, Gratton Y (1995) Respiratory activity and CO_2 production rates of microorganisms in the lower St. Lawrence Estuary. Cont Shelf Res 15: 613–631
Varma A, Palsson BO (1994) Stoichiometric flux balance models quantitatively predict growth and metabolic by-product secretion in wild-type *Escherichia coli* W3110. Appl Environ Microbiol 60:3724–3731
Walsh K, Koshland DE Jr (1984) Determination of flux through the branch point of two metabolic cycles. J Biol Chem 259:9646–9654
White A, Handler P, Smith EL (1964) Principles of biochemistry. McGraw-Hill, New York
Zirino A (1985) Mapping strategies in chemical oceanography. American Chemical Society, Washington, DC

Responsible Subject Editor: J. T. Hollibaugh, Tiburon, California, USA

Manuscript first received: October 23, 1995
Revised version accepted: April 28, 1996